JGR Space Physics

RESEARCH ARTICLE
10.1029/2021JA030153

Key Points:

- A 1D radial diffusion model with charge exchange loss is used to simulate the long-term evolution of ring current protons
- The energy-dependent transport, acceleration, and decay of >30 MeV/G ring current protons are generally well reproduced at $L^* \gtrsim 4$
- Some of the prompt losses at high L^* are captured by outward radial diffusion in the model, while others may due to additional loss mechanisms

Correspondence to:
X. Lyu,
xl0028@mix.wvu.edu

Citation:
Lyu, X., & Tu, W. (2022). Modeling the dynamics of energetic protons in Earth's inner magnetosphere. *Journal of Geophysical Research: Space Physics*, *127*, e2021JA030153. https://doi.org/10.1029/2021JA030153

Received 23 NOV 2021
Accepted 1 MAR 2022

Modeling the Dynamics of Energetic Protons in Earth's Inner Magnetosphere

Xingzhi Lyu[1] and Weichao Tu[1]

[1]Department of Physics and Astronomy, West Virginia University, Morgantown, WV, USA

Abstract Recently, Van Allen Probes data have revealed the interesting energy-dependent dynamics of energetic protons in Earth's inner magnetosphere. To quantify the role of radial diffusion and charge exchange to the observed energy-dependent dynamics of ring current protons, a 1D radial diffusion model with charge exchange loss is implemented. The observed proton flux over the long-term period of November 2012 to September 2013 is first converted to phase space densities, which are then simulated by our model driven by an outer boundary condition at $L^* = 5.5$ derived from the data. The simulation results show that our model generally captures the transport and acceleration of energetic protons at $\mu = 30$, 50, and 80 MeV/G and $K = 0.11\ G^{1/2}\ R_E$, suggesting that radial diffusion is the dominant source mechanism for >75 keV protons at $L^* = 3.5$–5.5. In addition, the observed fast decay of protons at lower μ and slow decay at higher μ are well captured by the model, demonstrating the dominant role of charge exchange in explaining the observed energy-dependent proton decay. For higher μ protons, prompt losses of protons on the time scale of hours are observed over a wide range of L^*, which is too fast to be explained by charge exchange. Some of the prompt losses at high L^* regions are reproduced by the model with outward radial diffusion to the outer boundary. However, many prompt losses observed at lower L^* regions are not captured by the model, which could be due to other loss mechanisms including electromagnetic ion cyclotron wave scattering and field line curvature scattering.

1. Introduction

The ring current, an electric current flowing toroidally in near-Earth space, plays a crucial role in the morphology and dynamics of the Earth's magnetosphere (Daglis et al., 1999). Changes in this current are responsible for the decreases of the Earth's surface magnetic field and can be characterized by the Dst index (e.g., Berko et al., 1975; Daglis et al., 1993; Sugiura, 1964; Williams, 1981). Energy density of the ring current is mainly carried by ~1 keV to a few hundred keV ions, most of which are protons during quiet times (i.e., prestorm and poststorm phases) (e.g., Krimigis et al., 1985; Zhao et al., 2015). Thus, modeling the long-term evolution of energetic protons is critical to obtaining a physical understanding of the ring current dynamics.

Previous studies have shown that injection (or convection) and radial diffusion are the two major source mechanisms for the transport and acceleration of ring current ions, but it is still under active debate which mechanism is more dominant. For example, Sheldon and Hamilton (1993) used the standard radial diffusion model combined with two non-adiabatic loss mechanisms to study the transport of ring current particles observed by Active Magnetospheric Particle Tracer Explorers/Charge Composition Explorer spacecraft. Their results showed good agreement with the data at ion energies greater than 30 keV and at $L > 4$, which suggests that for energetic ions radial diffusion is the main transport and acceleration mechanism that leads to the flux enhancement of ring current ions. Meanwhile, Gkioulidou et al. (2014, 2015) investigated small-scale ion injections using data from the Van Allen Probes/RBSPICE instrument during ring current buildups and found that injections could make a substantial contribution to the enhancement of ring current. Recently, Gkioulidou et al. (2016) studied the long-term pressure evolution of ring current protons using Van Allen Probes data and found that the proton dynamics are quite energy-dependent. They concluded that for lower energy protons (<80 keV) convection is the dominant mechanism for transport and acceleration, while for higher energy protons (>100 keV) radial diffusion is more dominant.

Several different mechanisms could also contribute to the loss of ring current protons. The major ones during geomagnetically quiet periods include coulomb scattering and charge exchange. Among these two mechanisms, charge exchange is the dominant loss process for ring current protons over most of the ring current energy range and it has been widely studied (e.g., Fok et al., 1991; Hamilton et al., 1988; Kistler et al., 1989). The charge

exchange lifetimes for ring current protons are strongly energy dependent, which are of about 1 day for equatorially mirroring protons at energies <75 keV and increasing rapidly to around hundreds of days at 200 keV (Liemohn, 1961, Jordanova et al., 1996; Smith & Bewtra, 1978). Other non-adiabatic mechanisms such as pitch angle scattering by the electromagnetic ion cyclotron (EMIC) waves (e.g., Jordanova et al., 2001; Khazanov et al., 2007), loss to the magnetopause by outward radial diffusion (e.g., Keika et al., 2005; Tu et al., 2019; Turner et al., 2014), field line curvature (FLC) scattering (e.g., Ebihara et al., 2011; Eshetu et al., 2021), and by bounce-drift resonant interaction with ULF waves (selectively for oxygen ions) (e.g., Li et al., 1993) could also play an important role in the fast loss of ring current ions during storm times. For example, Jordanova et al. (2001) modeled the proton precipitation caused by EMIC waves during a geomagnetic storm of 14–16 May 1997. The global pattern from their results shows that the precipitation was first located at higher L shells during prestorm conditions, moving to lower L shells in the storm main phase, and then receding back to higher L shells during the recovery phase. Turner et al. (2014) examined the evolution of flux versus L^* profiles for both MeV electrons and >100s keV protons during the 30 September 2012 storm and found concurrent dropout of energetic electrons and protons at $L^* > 4$ with features that are highly consistent with loss to the compressed magnetopause combined with outward radial diffusion. Eshetu et al. (2021) quantified the effect of the FLC scattering on ring current ions using test particle simulations under the T89c magnetic field model and found that for $Kp = 6$ the lifetime of 100 keV protons can be <10 hr at $L > 5$, while for 300 keV ions, the lifetime can be <10 hr at $L < 3.8$, and for stronger storms it could lead to fast loss even further inside. All these three mechanisms could lead to losses on timescales of hours, which are much faster than the loss by charge exchange especially for 100s keV protons.

Based on our discussions above, radial diffusion can play an important role in both the transport, acceleration, and loss of ring current protons, but its relative role compared to other mechanisms has not been well quantified. Using the unprecedented Van Allen Probes data with high energy resolution, we will apply a simple radial diffusion model with charge exchange loss to quantify the relative contribution of radial diffusion and charge exchange to the energy-dependent transport, acceleration, and loss of ring current protons (e.g., as reported in Gkioulidou et al. (2016)). In Section 2, we discuss the long-term observations of proton flux variations observed by Van Allen Probes and analyze the observed timescales of both decay and fast drop of energetic protons. Then, in Section 3 we introduce the 1D radial diffusion model and discuss the simulation results of the proton phase space densities (PSDs) at different μ values. Finally, conclusions and discussions on the results and future work are summarized in Section 4.

2. Observations and Data Analysis

2.1. Long-Term Variations of Ring Current Proton Fluxes

Ion fluxes (with no composition discrimination) measured by the Magnetic Electron Ion Spectrometer (MagEIS) instrument (Blake et al., 2013; Claudepierre et al., 2021) on Van Allen Probes with energies of ~60 keV–1 MeV from November 2012 to September 2013 (a 10-month period) are used in this study. Since previous works show that protons serve as the main carrier of ring current energy density during quiet times and small geomagnetic storms (e.g., Daglis et al., 1993; Krimigis et al., 1985), in this work we assume the measured ion fluxes are dominated by protons which is reasonable for long-term studies (e.g., Zhao et al., 2015). Issues with the MagEIS proton data have been reported on the RSBP ECT data website (https://rbsp-ect.newmexicoconsortium.org/science/DataQualityCaveats.php), but the energetic proton fluxes during the period studied in this work are generally in agreement with the RBSPICE data from Van Allen Probes (e.g., Gkioulidou et al., 2016; Zhao et al., 2015).

Figure 1 shows the proton fluxes at different energies of 70, 100, 190, 300, and 480 keV in the top five panels as a function of time and dipole L, measured by MagEIS on the Van Allen Probe-A from November 2012 to September 2013, along with the Dst index in the bottom panel. The observed proton fluxes exhibit energy-dependent dynamics during storm time. For lower energy protons (70–100 keV), the fluxes show fast transport across a wide range of L, followed with fast decay. While for higher energy protons (>100 keV), the fluxes are gradually enhanced at lower L, followed with slow decay. In addition, some prompt losses of higher-energy protons (>100 keV) are observed at both high and low L regions. The energy-dependent acceleration and loss timescales can be seen more clearly in Figure 2, where the observed flux at given L shells of $L = 5.0, 4.5, 4.0$, and 3.5, respectively are shown in the top five panels. In each panel, the fluxes are plotted versus time with different colors corresponding to different energies. By comparing to the Dst index variation in the bottom panel, we find the lower energy protons (70–100 keV) show fast increases in the storm main phase and then fast decay during

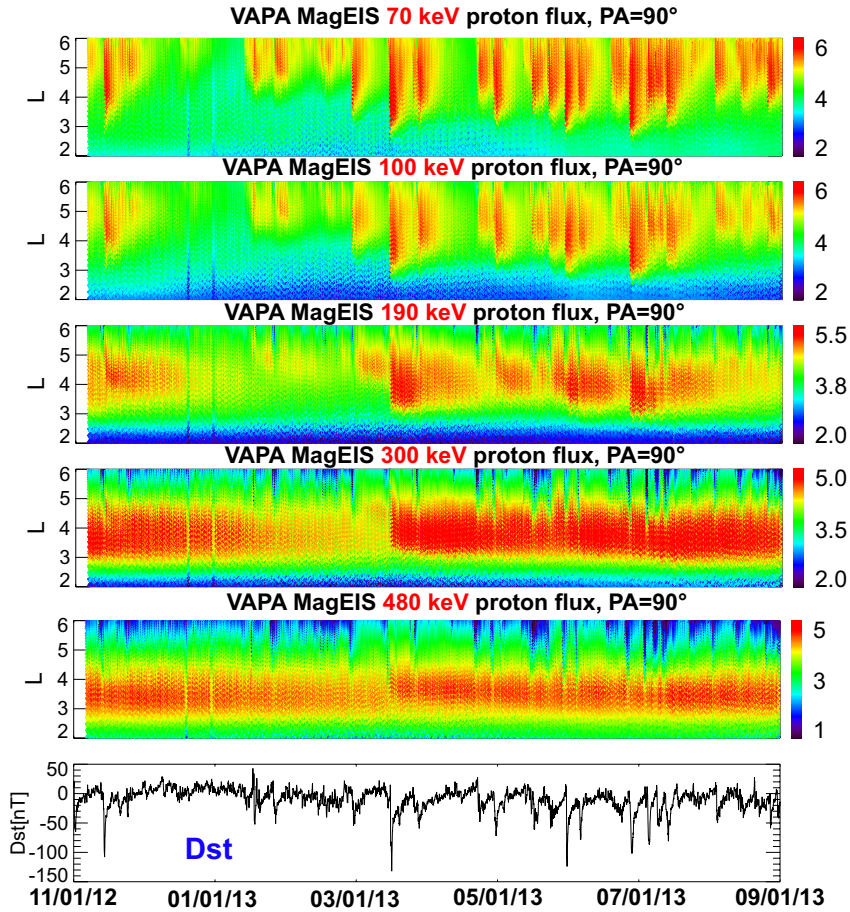

Figure 1. Proton fluxes (in units of $(cm^2\ s\ sr\ keV)^{-1}$) at energies of 70, 100, 190, 300, and 480 keV from November 2012 to September 2013, measured by Magnetic Electron Ion Spectrometer instruments onboard Van Allen Probe A, along with the Dst index.

the recovery phase. On the other hand, higher energy protons (>100 keV) often illustrate prompt losses during the main phase especially at higher L regions, and gradual recovery or even enhancement in the storm recovery phase. This energy-dependent dynamic is consistent with the findings of Gkioulidou et al. (2016), who suggest that for lower energy protons injection is the dominant transport and acceleration mechanism, while for >100 keV protons radial diffusion is more dominant. Here we would like to quantify how much of the observed transport and acceleration of energetic protons can be reproduced by radial diffusion and the role of charge exchange in explaining the observed energy-dependent decay of ring current protons.

2.2. Decay Analysis

To investigate the contribution of charge exchange to the fast decay of lower energy protons and slow decay of higher energy protons, we analyze the observed decay timescales of 70 and 300 keV protons by calculating the e-folding lifetimes of protons at these two energies at given L shells with results shown in Figure 3. Panel (a) plots the daily averaged fluxes of 70 keV (left column) and 300 keV (right column) protons from Van Allen Probes A for the 10-month period, and with panels (b–e) showing fluxes versus time at given L shells of $L = 5.0$, 4.5, 4.0, and 3.5, respectively. The observed decay interval of protons at a given L is then fitted with a function of $f = f_o e^{-t/\tau}$, where f is the proton flux at given energy and L which starts at value f_o and decay in time with e-folding lifetime τ. The best-fit exponential decay curve for each decay interval is marked as a red line in the figure with the fitted value of e-folding lifetime in unit of days denoted as a red number by each curve. To compare the observed decay lifetimes with the proton lifetimes due to charge exchange, we used the empirical formula given as (e.g., Fok et al., 1991; Liemohn, 1961):

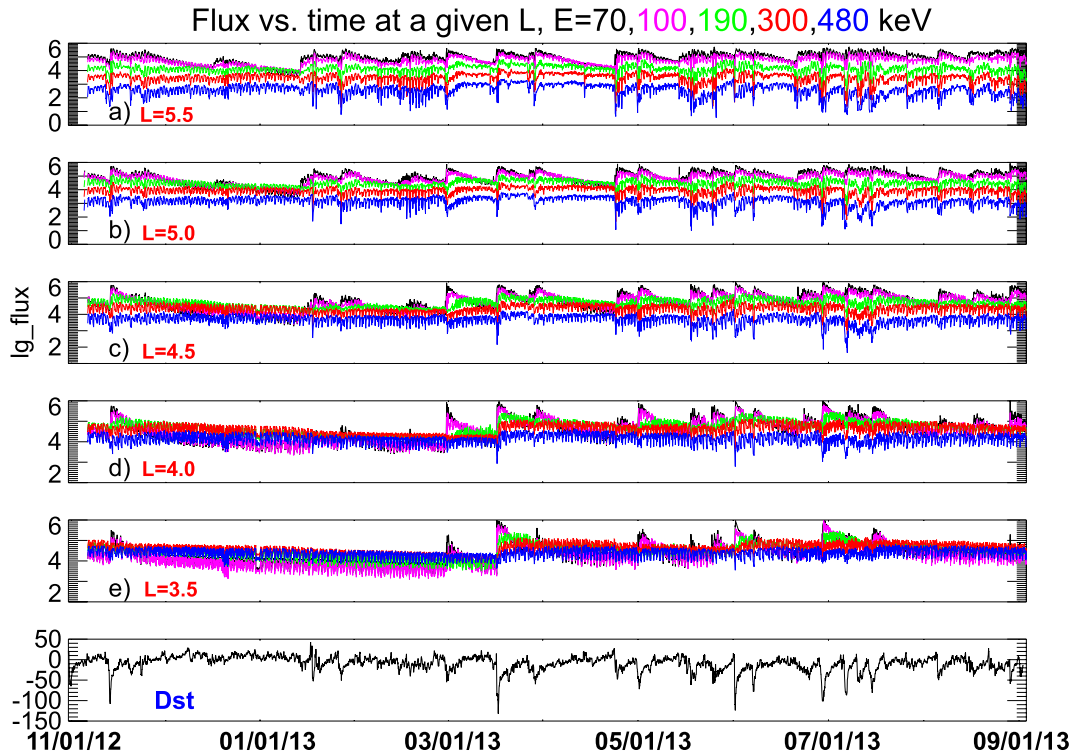

Figure 2. Proton fluxes (in units of $(\text{cm}^2\ \text{s sr keV})^{-1}$) at energies of 70 keV (black), 100 keV (magenta), 190 keV (green), 300 keV (red), and 480 keV (blue) at given L shells of (a) $L = 5.5$, (b) $L = 5.0$, (c) $L = 4.5$, (d) $L = 4.0$, and (e) $L = 3.5$ from November 2012 to September 2013, measured by Magnetic Electron Ion Spectrometer instruments onboard Van Allen Probe A, with the Dst index (nT) in panel (f).

$$\tau_e = \left(\sigma n_e^{(H)} v\right)^{-1} \tag{1}$$

where τ_e is the charge exchange lifetime for proton mirroring at the equator, σ is the charge exchange cross section, $n_e^{(H)}$ is the number density of neutral hydrogen, and v is the velocity of the ring current species. Among these, the neutral hydrogen density is obtained by Chamberlain model with the expression in terms of density at the exobase, N_c, and a partition function, ζ, as follows (Smith & Bewtra, 1978):

$$n_e^{(H)}(r) = N_c\, e^{-\left(\lambda_c - \lambda(r)\right)} \zeta(\lambda) \tag{2}$$

where N_c and the λ_c are expressed by assuming the exobase to be at 500 km with $N_c = 4 \times 10^4\ \text{cm}^{-3}$ and $\lambda_c = 5.82$. $\lambda(r) = \frac{1.0785\,\lambda_c}{r/R_E}$ where R_E is the Earth radius, and the partition function is given by:

$$\zeta(\lambda) = \frac{2}{\sqrt{\pi}}\gamma\left(\frac{3}{2}, \lambda\right) + \frac{1}{\sqrt{\pi}}\left[\frac{\sqrt{\pi}}{2} - \gamma\left(\frac{3}{2}, \lambda\right) - \frac{\left(\lambda_c^2 - \lambda^2\right)^{\frac{1}{2}}}{\lambda_c} e^{-\psi_1}\left(\frac{\sqrt{\pi}}{2} - \gamma\left(\frac{3}{2}, \lambda - \psi_1\right)\right)\right] \tag{3}$$

where $\psi_1 = \lambda^2/(\lambda + \lambda_c)$ and γ is the incomplete Γ-function.

Our calculation shows that the charge exchange lifetime ranges from 1 to 2.6 days from $L = 3.5$ to 5 for 70 keV protons and ranges from 229 to 525 days from $L = 3.5$ to 5 for 300 keV protons. Therefore, our analyses show that the observed decay timescales for both 70 and 300 keV protons shown in Figure 3 are generally consistent with the empirical values of charge exchange lifetimes, suggesting that charge exchange plays a dominant role explaining the observed energy-dependent decay of energetic protons. However, a more detailed comparison between the observed and empirical lifetimes shows that the observed decay lifetimes for lower energy protons (e.g., 70 keV here) are two to four times longer than the empirical charge exchange lifetimes, while the observed decay lifetimes at higher energy (e.g., at 300 keV) are two to five times shorter. This also indicates that the empirical model

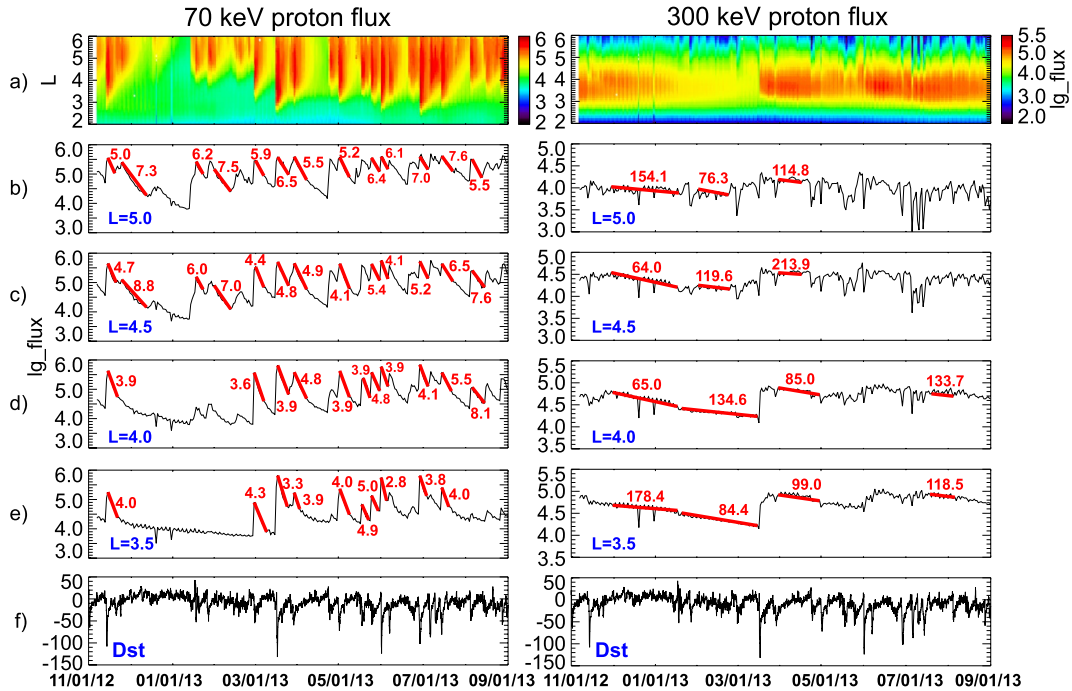

Figure 3. (a) Daily averaged fluxes (in units of $(cm^2\ s\ sr\ keV)^{-1}$) of ~70 keV (left column) and 300 keV (right column) protons from November 2012 to September 2013, measured by Magnetic Electron Ion Spectrometer instrument on Van Allen Probe A. (b–e) Fluxes of 70 keV (left column) and 300 keV (right column) protons at given $L = 5.0$, 4.5, 4.0, and 3.5, respectively, red numbers are the fitted e-folding lifetimes (in days) for the decays (red solid lines). (d) Dst index (nT) for the time period.

for charge exchange lifetimes may have some uncertainties, which motivates us to introduce a free parameter in the charge exchange loss term in our model as discussed in Section 3.1.

2.3. Fast Drop Analysis

For higher energy protons (>100 keV), prompt losses of proton fluxes are observed during storm main phase as shown in Figure 2 and discussed therein. Here we pick two storms to analyze the loss timescales for the fast drop of high-energy protons with results shown in Figure 4. For the long-term flux variations and decay analysis, we have only used flux data from Van Allen Probe-A; to estimate the timescales more accurately for the fast drop, fluxes data from both Van Allen Probes are included in the analysis. Figures 4a–4d show the observed proton fluxes for the two storms at given L shells of $L = 5.0$, 4.5, 4.0, and 3.5, respectively, with different colors in each panel showing fluxes at different energies of 190, 300, and 480 keV. Flux data from both probes are used, with the plus signs representing data from Probe A, and the asterisk signs denoting data from Probe B. Panel (e) shows the L variation of Probe A (in black) and B (in red) during Strom 1 (left column) and Storm 2 (right column), and with the Dst index for both storms shown in panel (f). The proton loss timescales for the observed fast drop during both storms are estimated using the e-folding lifetime fitting described in Section 2.2 over the intervals between the two dash lines marked in each panel for different L and energies. The estimated values of fast drop timescales are listed in the tables at the bottom of the figure.

Overall, the results in the two tables show that the observed fast drop for both storms occurs on the timescale of hours which is too fast to be explained by charge exchange. The energy and L dependence of the estimated lifetimes may shed some lights on the potential loss mechanisms. For example, for storm #1 the fast drop at a fixed energy is shown to be generally faster at higher L, which is consistent with the loss by outward radial diffusion to the magnetopause. The drop timescale of storm #1 also shows an interesting energy dependence at fixed L values with faster loss at higher energies. This energy dependence is opposite to the energy dependence of radial diffusion coefficient suggested by Liu et al. (2016), with lower diffusion rate for higher energy particles (whose drift frequencies are higher corresponding to less power of the ULF waves that can be drift-resonant with the particles). However, the loss rate due to outward radial diffusion is not only related to the diffusion coefficient,

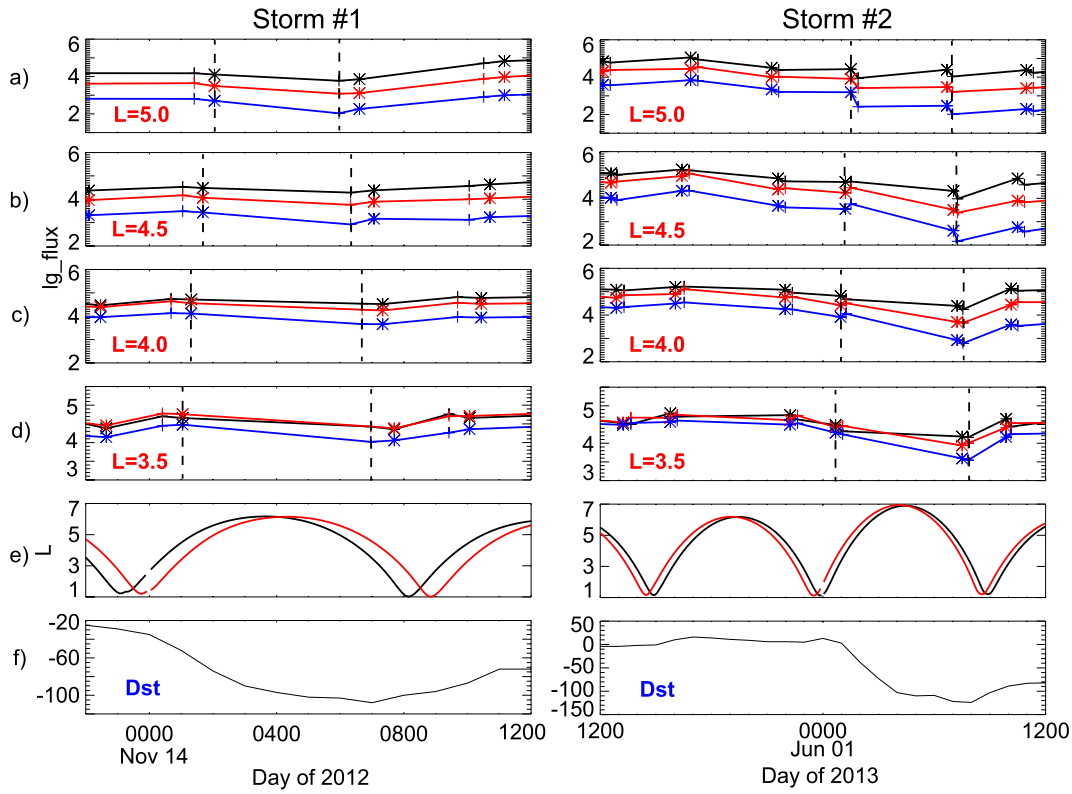

Prompt loss timescales (hours) of Storm #1

Storm #1	L=5.0	L=4.5	L=4.0	L=3.5
E=190 keV	5.1	10.1	13.1	11.2
E=300 keV	4.1	6.7	8.4	7.8
E=480 keV	2.6	3.9	5.1	5.6

Prompt loss timescales (hours) of Storm #2

Storm #2	L=5.0	L=4.5	L=4.0	L=3.5
E=190 keV	6.0	3.6	5.0	9.4
E=300 keV	3.4	3.1	3.8	7.3
E=480 keV	2.0	1.9	2.5	4.2

Figure 4. Fluxes (in units of $(cm^2\ s\ sr\ keV)^{-1}$) of 190 keV (black), 300 keV (red), and 480 keV (blue) protons at L = (a) 5.0, (b) 4.5, (c) 4.0, and (d) 3.5, measured by Magnetic Electron Ion Spectrometer on Van Allen Probe A ("+") and B ("∗") for storm 1 (left column) and storm 2 (right column). (e) L values of Van Allen Probe A (black) and B (red). (f) Dst index (nT) of two storms. Two vertical dashed lines in each panel indicate the time intervals used to estimate the fast drop timescales show in the bottom table.

but also dependent on the L^* gradient of the proton PSDs. Therefore, it is interesting to investigate how much of the observed fast drop during storm #1 could be accounted for by outward radial diffusion, which will be discussed in Section 3.3. Other loss mechanisms could also contribute to the fast drop observed in storm #1, such as FLC scattering which is more efficient for higher energy protons at higher L regions (Eshetu et al., 2021). For storm #2, the estimated drop timescales shown in the right table suggest that the drop is observed to be faster at higher energies, but with the fastest loss at a localized L ($L = 4.5$), which is consistent with the picture of localized particle scattering loss by EMIC waves.

3. Simulations

3.1. Model Description

To quantitatively study how much radial diffusion and charge exchange can reproduce the dynamics of energetic protons in the ring current, here we implement a 1-D radial diffusion model based on the Fokker-Planck equation (Schulz & Lanzerotti, 1974):

$$\frac{\partial f}{\partial t} = L^2 \frac{\partial}{\partial L}\left(\frac{D_{LL}}{L^2}\frac{\partial f}{\partial L}\right) - \frac{f}{\tau} \tag{4}$$

where L is Roederer L^* which is inversely proportional to the third adiabatic invariant (Roederer, 1970), $f(L,t)$ is the proton PSD in unit of (c/MeV/cm)^3 at fixed μ and K values, D_{LL} is the radial diffusion coefficient, and τ is the proton lifetime which only includes the charge exchange loss in this model. For the radial diffusion coefficient, we adopt the empirical formula of the electric diffusion coefficient D_{LL}^E from Liu et al. (2016) shown in Equation 5 below, since many studies have suggested the electric diffusion coefficient is dominant over the magnetic diffusion coefficient (e.g., Ozeke et al., 2014; Tu et al., 2012):

$$D_{LL} = A_0 \cdot 1.115 \cdot 10^{-6} \cdot 10^{0.281 \times Kp} \cdot L^{8.184} \cdot \mu^{-0.608} \tag{5}$$

A free parameter A_0 is introduced in Equation 5 of D_{LL} to account for the uncertainties of the empirical model, following the method in Tu et al. (2009). The unit of μ in Equation 5 is MeV/G and the diffusion coefficient D_{LL} is in unit of day^{-1}. The charge exchange proton lifetime τ is constructed based on the empirical formula from Smith and Bewtra (1978), specified as:

$$\tau = \tau_0 \cdot \tau_e \cos^{3.5\pm0.2} \lambda_m \tag{6}$$

where τ_e is the charge exchange lifetime for protons mirroring at the equator (given by Equation 1 above), λ_m is the mirror latitude of protons, and τ_0 is another free parameter introduced to account for the uncertainties of the empirical lifetime model. τ is in unit of days.

Simulations using our model are performed for the entire period from November 2012 to September 2013. The model outer boundary is set at $L^* = 5.5$, and the proton PSD data observed by Van Allen Probes A and B (discussed in detail in Section 3.2 below) are used to derive the time-dependent outer boundary condition. The initial condition of the model is also specified using the proton PSD data averaged over the first day of the simulation interval for $L^* = 3.5$–5.5. The free parameters in the model, A_0 and τ_0, are determined by maximizing the prediction efficiency (PE) from the model defined as (Li et al., 2001):

$$\mathrm{PE} = 1 - \frac{\sum_i^n (d_i - p_i)^2}{\sum_i^n \left(d_i - \bar{d}\right)^2} \tag{7}$$

where d_i and p_i are the observed and modeled proton PSD, respectively, and $\bar{d}$ is the average value of all d_i. PE = 0 means the model results are as good as the averaged data, and PE = 1 means perfect modeling. The model has better performance as PE gets closer to one.

3.2. Long-Term Variations of Proton PSD Data

The observed variations of proton fluxes are controlled by both adiabatic (i.e., Dst effect (Li et al., 1997)) and non-adiabatic processes. To focus on the non-adiabatic variations of energetic protons, we convert the long-term proton flux data measured by the MagEIS instrument aboard Van Allen Probes A and B into PSDs (Chen et al., 2005) as a function of the three adiabatic invariants (μ, K, and L^*) in the Tsyganenko 04 storm time model (TS04) (Tsyganenko & Sitnov, 2005). Figure 5 shows the calculated PSD as a function of time and L^* at $K = 0.11$ G$^{1/2}R_E$ and $\mu = 30$, 50, and 80 MeV/G respectively in the top three panels, with the Dst index shown in the bottom panel. $\mu = 30$, 50, and 80 MeV/G correspond to proton energies of ~120 keV, 200 and 330 keV at $L^* = 4.5$ respectively and correspond to overall >75 keV protons over the range of $L^* = 3.5$–5.5. It is clear that the PSD data in all the three panels show a generally positive gradient versus L^* which suggests the important role of radial diffusion in the observed dynamics. Similar to the flux dynamics discussed in Section 2, fast decay in proton PSD is observed at $\mu = 30$ MeV/G, with slower decay for higher μ protons, which is consistent with the energy dependence of charge exchange loss. In addition, prompt losses in proton PSD are observed at both higher and lower L^* for higher μ protons (e.g., $\mu = 50$ and 80 MeV/G). Using these PSD data to specify the outer boundary and initial conditions of the model, we perform the long-term simulations of proton PSD variations at $\mu = 30$, 50, and 80 MeV/G with the results shown in the next section.

3.3. Model Results

Figure 6 shows the model results at $\mu = 30$ MeV/G and $K = 0.11$ G$^{1/2}$ R_E. Panel (a1) plots the PSD data versus time and L^*, which is identical to the top panel of Figure 5. Panel (a2) plots the model results with the maximum

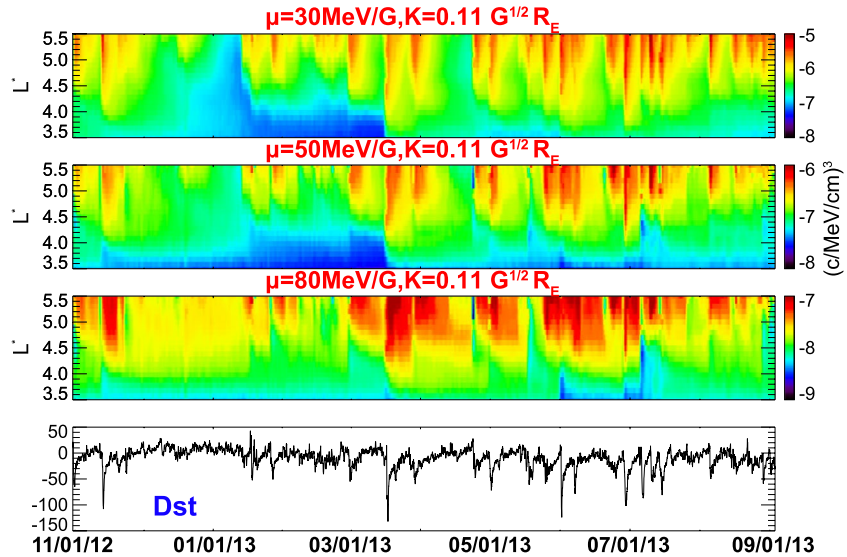

Figure 5. Proton phase space densities data (in unit of [c/MeV/cm]^3) for μ = 30, 50, and 80 MeV/G and $K = 0.11$ G$^{1/2}$ R_E from November 2012 to September 2013 along with the Dst index (nT) at the bottom panel.

PE value and the corresponding best-fit free parameters shown in the first row of Table 1. We have also calculated the linear correlation coefficient between the data and model results which is shown as the LC value in the table. The log difference between the model and the data are presented in panel (a3), with an overplotted black

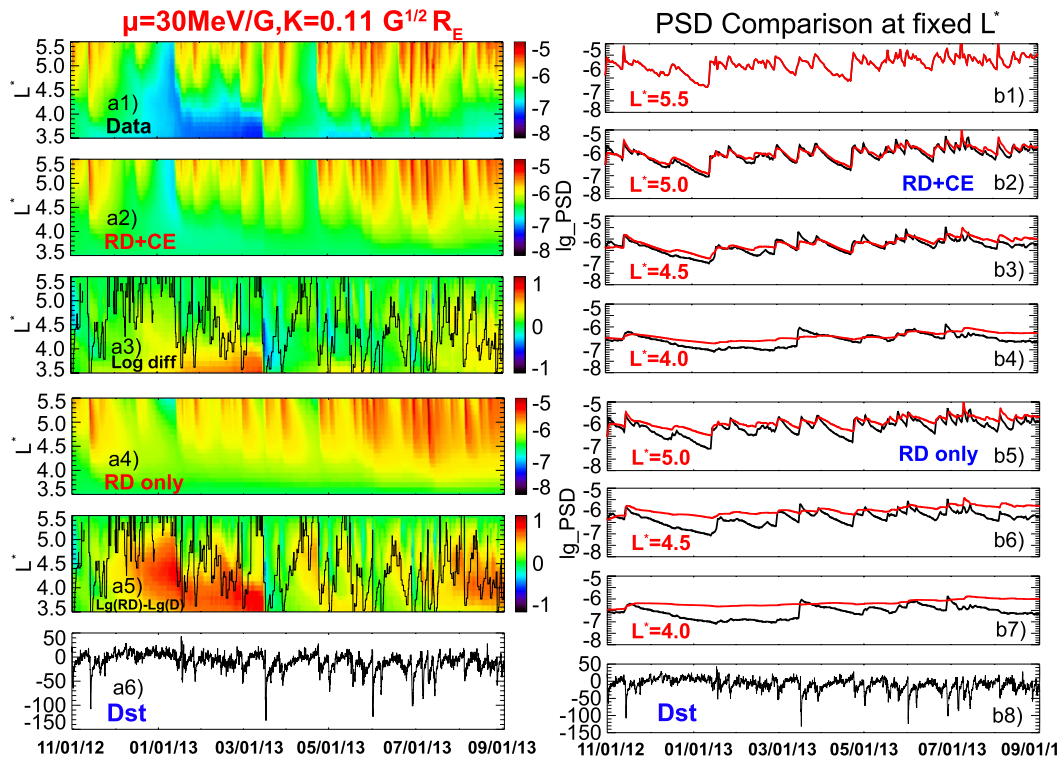

Figure 6. (a1 and a2) Proton phase space density data in unit (c/MeV/cm)^3 and simulation results at $\mu = 30$ MeV/G and $K = 0.11$ G$^{1/2}$ R_E. (a3) Log difference between model and data, lg (model)-lg (data), with the black line showing the location of the plasmapause. (b1–b4) Comparison between data (black curve) and model results (red curve) at given $L^* = 5.5$, 5.0, 4.5, and 4.0, respectively. (a4 and a5) radial diffusion only model results and the log difference of it to data. (b5–b7) Comparison between data and radial diffusion only results at each given L^*. (a6 and b8) Dst index (nT).

Table 1
Best Fitting Parameters for Runs of μ = 30, 50, and 80 MeV/G

Run (RD + CE)	A_0	τ_0	PE	LC
μ = 30 MeV/G	2.98	0.76	0.83	0.91
μ = 50 MeV/G	2.24	0.37	0.79	0.89
μ = 80 MeV/G	1.02	0.06	0.70	0.84

curve showing the location of the plasmapause calculated using the empirical model from O'Brien and Moldwin (2003):

$$L_{pp} = -1.57\log_{10}|\mathrm{Dst}^*| + 6.3 \quad (8)$$

where Dst* is the minimum value of Dst (in unit of nT) during the previous 24 hr. The generally good match between panels (a1) and (a2) and the higher PE and LC values suggest that our model very well captures the transport, acceleration, and decay of energetic protons across all L^* at μ = 30 MeV/G, even though panel (a3) shows that there are overestimations from the model inside the plasmapause. $A_0 = 2.98$ and $\tau_0 = 0.76$ in the table means that to best reproduce the observed PSD dynamics, the model needs a radial diffusion coefficient that is ~3 times stronger than what is provided by the empirical model in Liu et al. (2016) and a charge exchange lifetime that is ~1.3 times faster than the value from the Smith and Bewtra (1978) empirical model. To better illustrate the model performance at different L^* shells, we take cuts of the data and model results at $L^* = 5.5$ (outer boundary), $L^* = 5.0$, 4.5, and 4.0, respectively, and plot the comparison in panels (b1–b4). Again, our model performs very well in capturing the fast enhancement and slow decay of protons at μ = 30 MeV/G over a wide range of L^*, even though for $L^* = 4.0$ (panel (b4)) the model misses a couple of strong enhancements that penetrate deeply in L^* (e.g., during the intense 17 March 2013 storm) and slightly overestimates the data during some decay intervals (e.g., after the major storm in November 2012).

Given that the observed decay of protons at μ = 30 MeV/G is well reproduced by our model with radial diffusion and charge exchange loss, it is useful to distinguish the relative contribution of charge exchange and outward radial diffusion to the data-driven outer boundary to the observed decay at different L^* regions. That is investigated here by turning off the charge exchange loss in the simulation and only keeping the radial diffusion (with the same value of $A_0 = 2.98$). Model results with radial diffusion only (RD only) and their comparison to the data are shown in panels (a4, a5 and b5–b7) for more detailed comparison at different L^* shells. We see that without charge exchange loss the model could not reproduce the fast decay of protons at μ = 30 MeV/G, leading to overestimation of the model at all L^* regions. These suggest that for μ = 30 MeV/G charge exchange is the dominant loss mechanism for the fast decay of protons, while radial diffusion is the dominating mechanism for the observed proton transport and acceleration.

Similar simulations are performed for higher μ protons at μ = 50, 80 MeV/G with results shown in Figure 7. Panels (a1–a3) show the PSD data, model results, and log difference between model and data versus time and L^* at μ = 50 MeV/G and $K = 0.11\ \mathrm{G}^{1/2}\ R_E$, while panels (b1–b4) on the right exhibit the comparison at each given L^*. The same configurations for μ = 80 MeV/G protons are plotted in panels (c1–c3 and d1–d4). The best fitting parameters for these two runs are also included in Table 1 (bottom two rows). From the comparisons to the data, we find that our model generally reproduces the transport and acceleration of protons over a wide range of L^*, suggesting the dominant role of radial diffusion in controlling these observed proton dynamics at higher μ values. Similar to the lower μ case shown in Figure 6b4, the higher μ results in Figures 7b3, 7b4, 7d3 and 7d4 show that some of the fast enhancements observed at low L^* regions are not well captured by the model (e.g., during the 17 March 2013 storm), potentially due to strong injections of proton which are not included in the model. The slower decay of higher μ protons observed in the data is also generally captured by the model with charge exchange, even though there is slight overestimation at low L^* regions similar to the lower μ results (e.g., Figure 7b4).

A notable difference in the PSD data as μ increases from Figures 6 and 7 is that prompt losses in PSD start to show up at both high and low L^* regions at higher μ values, which is clearly shown in the black PSD data curves in the right panels of Figure 7. Some of the prompt losses at high L^* are captured by the model, e.g., the PSD drop during the 14 November 2012 storm (storm #1 analyzed in Section 2.3 and marked in panels (b5) and (d5)) at $L^* = 5.0$ shown in panels (b2) and (d2), which suggests outward radial diffusion can somewhat account for the fast PSD drops observed at high L^* regions. However, many other PSD drops at lower L^* regions as shown in panels (b3, b4, d3, and d4) are not captured by the model, for example, the drop during the 1 June 2013 storm (storm #2 analyzed in Section 2.3 and marked in panels (b5 and d5)), which may be caused by other loss mechanisms such as EMIC wave scattering or FLC scattering not yet included in the model. It is also possible that due to

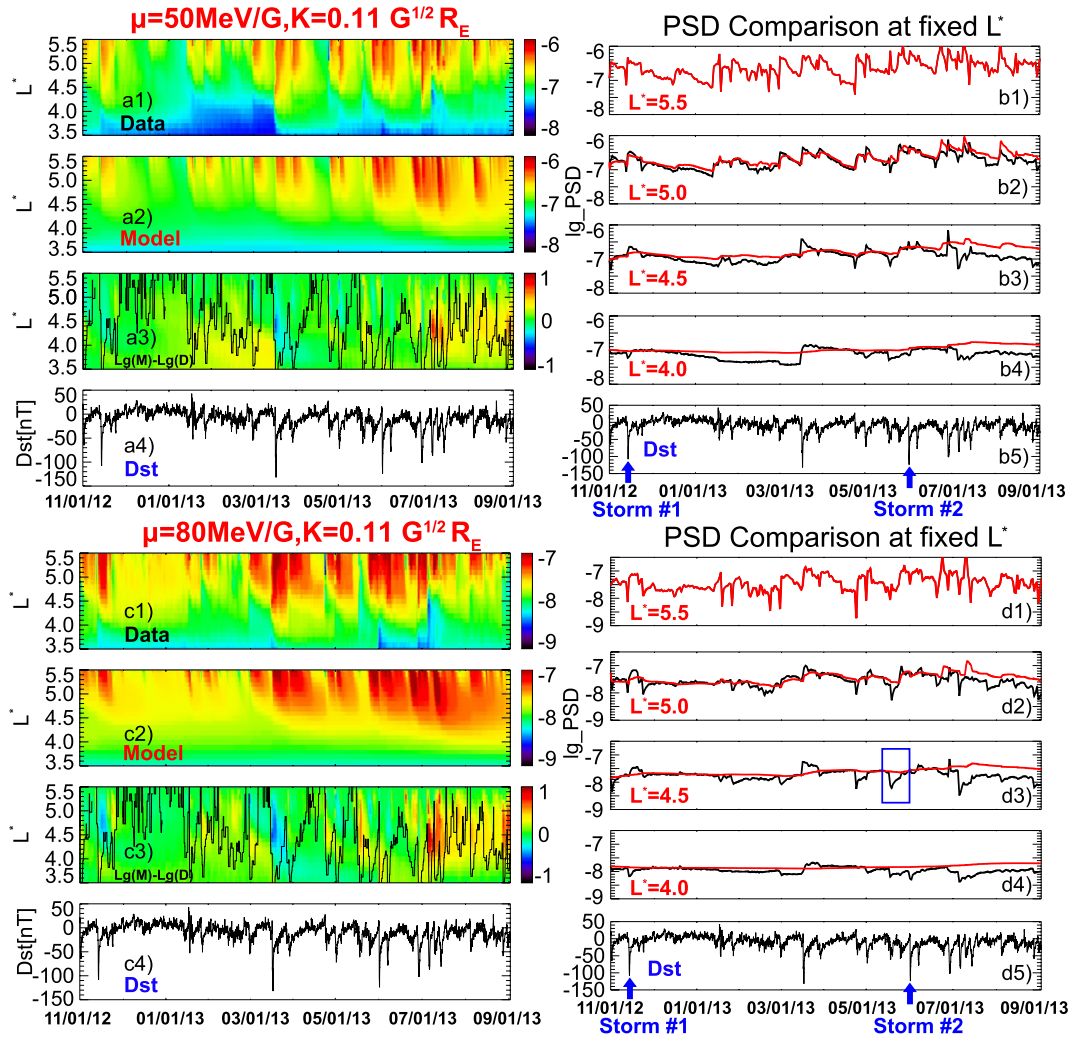

Figure 7. (a1 and a2) Proton phase space density (PSD) data and simulation results at $\mu = 50$ MeV/G and $K = 0.11$ $G^{1/2}$ R_E. (a3) Log difference between model and data. (b1–b4) Comparison between data (black curve) and model results (red curve) at given $L^* = 5.5$, 5.0, 4.5, and 4.0, respectively. (c1 and c3) PSD data and model result $\mu = 80$ MeV/G and the log difference between them. (d1–d4) Comparison between data and simulation results at each given L^*. (a4, c4, b5, d5) Dst index (nT).

imperfection of the TS04 magnetic field model, the adiabatic Dst effect was not completely removed in the PSD data calculation during the storm main phases when fast proton losses were observed.

Even though the model does not capture some of the fast PSD drops observed at low L^* regions, radial diffusion in the model still performs well in reproducing the general levels of proton PSD at lower L^* regions, including those recovered after the fast PSD drops (e.g., the boxed interval in Figure 7d3). An interesting question to ask is: if the fast drop was captured by the model, is radial diffusion still sufficient to enhance the proton PSD to the observed level? To investigate this, we pick the interval boxed in Figure 7d3 for $\mu = 80$ MeV/G protons at $L^* = 4.5$ and zoomed in the data model comparison in Figure 8a (with the data shown in plus symbols and model still in red). For comparison, we redo the simulation for this interval by manually inserting a drop in the modeled PSD over all L^* at the observed drop time with the observed drop level while keeping the radial diffusion at the same rate. Then the model is re-initialized at the observed drop time. The new model results in panel (b) show that even with the PSD drop included radial diffusion is still fast enough to transport and accelerate the protons to the observed level, well capturing the observed recovery of proton PSD.

Due to the miss of prompt losses at low L^* regions in the model, in Table 1 we see that the PE at higher μ values is generally lower than that at lower μ value. But they are still above 0.7 suggesting the general good performance

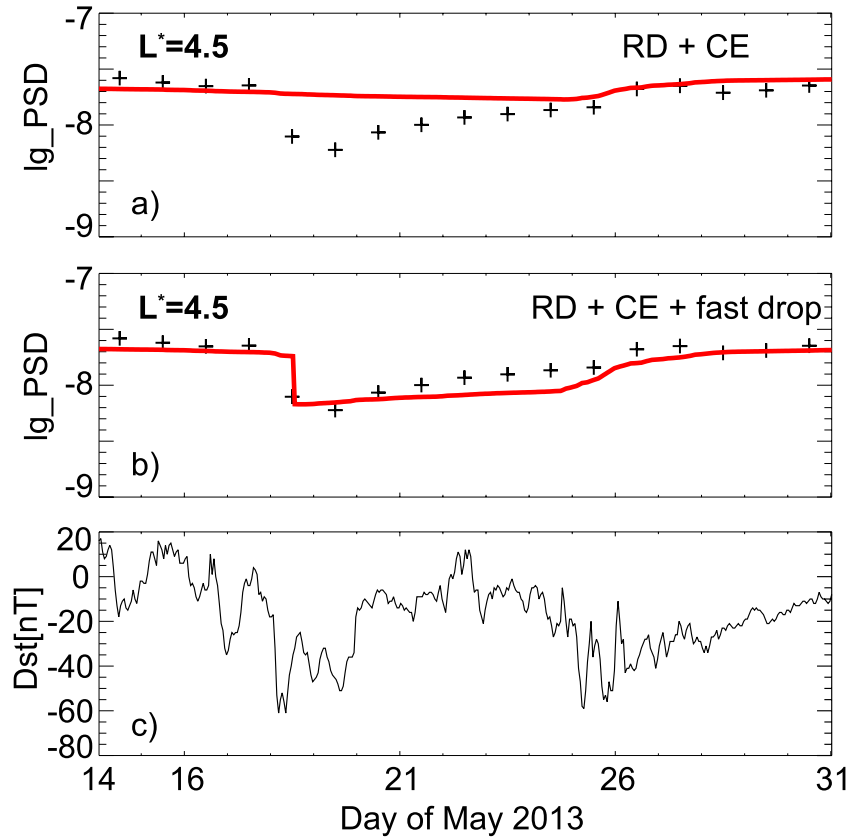

Figure 8. (a) Proton phase space density (PSD) data ("+") versus model results (Radial Diffusion + Charge Exchange, red curve) at $L^* = 4.5$ during 14–31 May 2013 (boxed in Figure 7d3). Panel (b) same as panel (a), but with the modeled PSD including a manually inserted fast drop. (c) Dst index (nT).

of the model over all the μ values and the dominant role of radial diffusion and charge exchange in explaining the transport, acceleration, and decay of energetic protons in the ring current. The best-fit values of A_0 are between 1 and 3 for all three runs and the best-fit values for τ_0 are all smaller than but generally close to 1, except for the highest μ run returning a best fit with a much smaller τ_0 value to try accounting for some of the observed prompt losses. These results suggest that to best match the observed PSD variations, a radial diffusion coefficient slightly higher than what is given by the Liu et al. (2016) empirical model and a charge exchange loss slightly faster than what is provided in the Smith and Bewtra (1978) empirical model is needed. But these two empirical models perform generally well in specifying the radial diffusion and charge exchange rates of ring current protons over the long-term period.

4. Conclusions and Discussions

Energy-dependent dynamics of energetic protons in Earth's inner magnetosphere were observed by the MagEIS instrument of Van Allen Probe A over the long-term period from November 2012 to September 2013. Lower energy proton (70–100 keV) exhibits fast enhancements across a wide range of L during the storm main phase, followed with fast decay in the recovery phase. On the other hand, higher energy protons (>100 keV) illustrate prompt losses during the main phase, followed with gradual recovery or increase during the recovery phase which then undergoes slow decay. By calculating the e-folding lifetimes of protons observed at different energies, we find that the observed decay timescales for both 70 and 300 keV protons are generally consistent with the empirical values of charge exchange lifetimes, showing that charge exchange plays a dominant role in the observed energy-dependent decay of energetic protons. We have also selected two storms to analyze the loss timescales for the observed prompt losses of high-energy protons (>100 keV) using fluxes observed by both Van Allen Probes. The results show that the observed prompt losses for both storms occur on the timescale of hours which is too fast

to be explained by charge exchange. The L and energy dependence of the estimated timescales suggests that the fast drop during storm #1 could be potentially caused by outward radial diffusion to the magnetopause, which is also confirmed by our modeling results discussed later in the paper (Section 3.3), while the fast drop during storm #2 is more consistent with the picture of EMIC wave scattering loss.

To quantitatively study the role of radial diffusion and charge exchange to the observed energy-dependent transport, acceleration, and loss of energetic protons, we calculated the proton PSD as a function of the three adiabatic invariants based on the flux data and implemented a 1-D radial diffusion model with charge exchange loss to simulate the proton dynamics. The calculated proton PSD at $K = 0.11$ G$^{1/2}$ R_E and $\mu = 30$, 50, and 80 MeV/G (which correspond to >75 keV protons at $L^* = 3.5$–5.5) generally shows a positive gradient versus L^*, which suggests the important role of radial diffusion in the observed transport and acceleration of protons. Similar to the energy-dependent loss shown in the flux data, lower μ proton PSD ($\mu = 30$ MeV/G) show fast decay in time, while higher μ protons ($\mu = 50$ and 80 MeV/G) decay at a slower rate but often illustrate prompt losses at both higher and lower L^* regions. The time-dependent proton PSD data at $L^* = 5.5$ is then used as the outer boundary condition to drive our long-term simulations of protons at $K = 0.11$ G$^{1/2}$ R_E and $\mu = 30$, 50, and 80 MeV/G, respectively. Two free parameters, A_0 and τ_0, are introduced to the empirical formulae of radial diffusion coefficient and charge exchange loss used in the model, whose values are determined by best fitting the model results to the observed PSD variations (i.e., maximizing PE). Overall, the general good match between the data and the model results and the higher PE and LC values for all three μ values suggest that our model very well captures the transport, acceleration, and decay of energetic protons at $\mu = 30$, 50, and 80 MeV/G over $L^* = 3.5$–5.5. Specifically, our simulation results show that:

1. Radial diffusion from the data-driven outer boundary could generally well explain the transport and acceleration of these energetic protons inside $L^* = 5.5$, even though some occasional strong enhancements of protons at low L^* regions are not captured by the model which may be caused by fast injections. Our results do not rule out the potentially importance of injections to the proton enhancements observed at the model outer boundary of $L^* = 5.5$. The best-fit values of A_0 are in the range of 1–3 for the three μ runs, which suggests that the radial diffusion coefficient from the Liu et al. (2016) empirical model performs generally well in specifying the radial diffusion coefficients of ring current protons over the long term, even though a slightly faster diffusion rate is preferred by the best fits.
2. Charge exchange loss in the model could generally account for the observed fast decay of low μ protons and slower decay of higher μ protons, even though there was some overestimation from the model at low L^* regions (generally inside the plasmapause). The best-fit values of τ_0 for the three μ runs are generally close to 1, which suggests that the charge exchange proton lifetimes specified by the Smith and Bewtra (1978) empirical model perform generally well over the long-term period, even though loss rates slightly faster than the empirical values are preferred by the best fits.
3. For higher μ protons ($\mu = 50$ and 80 MeV/G), some of the prompt losses at higher L^* could be explained by the model (e.g., storm #1), which suggests the important role of outward radial diffusion to the fast PSD drops observed at high L^* regions. Many prompt losses at lower L^* are not captured by the model (e.g., storm #2), which are potentially caused by other loss mechanisms including EMIC wave scattering and FLC scattering. To study the influence of the prompt losses that are missed by the model, we have manually inserted a fast drop in the model for a selected interval. The simulation results show that radial diffusion is still sufficient to enhance the proton PSD to the observed level after the drop, which further demonstrates the dominant role of radial diffusion to the transport and acceleration of energic protons at even low L^* regions. To better capture the fast proton drops in our model, the effects from the EMIC wave scattering (e.g., Jordanova et al., 2001) and FLC scattering loss (e.g., the empirical model from Eshetu et al. (2021)) will need to be included in the future.

Data Availability Statement

Van Allen Probes MagEIS data used in this paper are available from the ECT Science Operations and Data Center (https://www.rbsp-ect.lanl.gov/data_pub/). Geomagnetic activity indices were obtained from the NASA OMNIWeb (http://cdaweb.gsfc.nasa.gov). PSD data used in the study are deposited on the data repository https://doi.org/10.5281/zenodo.5721475, which is publicly available.

Acknowledgments
This work was supported by the NASA grants 80NSSC18K1284, 80NSSC19K0908, and 80NSSC19M0146, the DOE grant DE-SC0020294, NSF Grant AGS 1752736, and the Cottrell Scholar Award ID No. 25883.

References

Berko, F. W., Cahill, L. J., Jr., & Fritz, T. A. (1975). Protons as the prime contributors to storm time ring current. *Journal of Geophysical Research*, *80*(25), 3549–3552. https://doi.org/10.1029/JA080i025p03549

Blake, J. B., Carranza, P. A., Claudepierre, S. G., Clemmons, J. H., Crain, W. R., Dotan, Y., et al. (2013). The Magnetic Electron Ion Spectrometer (MagEIS) instruments aboard the radiation belt storm probes (RBSP) spacecraft. *Space Science Reviews*, *179*(1–4), 383–421. https://doi.org/10.1007/s11214-013-9991-8

Chen, Y., Friedel, R. H. W., Reeves, G. D., Onsager, T. G., & Thomsen, M. F. (2005). Multisatellite determination of the relativistic electron phase space density at geosynchronous orbit: Methodology and results during geomagnetically quiet times. *Journal of Geophysical Research*, *110*(A10), A10210. https://doi.org/10.1029/2004JA010895

Claudepierre, S. G., Blake, J. B., Boyd, A. J., Clemmons, J. H., Fennell, J. F., Gabrielse, C., et al. (2021). The magnetic electron ion spectrometer: A review of on orbit sensor performance, data, operations, and science. *Space Science Reviews*, *217*, 80. https://doi.org/10.1007/s11214-021-00855-2

Daglis, I. A., Sarris, E. T., & Wilken, B. (1993). AMPTE/CCE observations of the ion population at geosynchronous altitudes. *Annals of Geophysics*, *11*, 685–696.

Daglis, I. A., Thorne, R. M., Baumjohann, W., & Orsini, S. (1999). The terrestrial ring current: Origin, formation, and decay. *Review sssof Geophysics*, *37*(4), 407–438. https://doi.org/10.1029/1999RG900009

Ebihara, Y., Fok, M.-C., Immel, T. J., & Brandt, P. C. (2011). Rapid decay of storm time ring current due to pitch angle scattering in curved field line. *Journal of Geophysical Research*, *116*(A3), A03218. https://doi.org/10.1029/2010JA016000

Eshetu, W. W., Tu, W., Jordanova, V. K., & Cowee, M. (2021). Quantifying the effect of magnetic field line curvature scattering on the loss of ring current ions. *Journal of Geophysical Research: Space Physics*, *126*(1), e2020JA028497. https://doi.org/10.1029/2020JA028497

Fok, M. C., Kozyra, J. U., Nagy, A. F., & Cravens, T. E. (1991). Lifetime of ring current particles due to Coulomb collisions in the plasmasphere. *Journal of Geophysical Research*, *96*(A5), 7861. https://doi.org/10.1029/90ja02620

Gkioulidou, M., Ohtani, S., Mitchell, D. G., Ukhorskiy, A. Y., Reeves, G. D., Turner, D. L., et al. (2015). Spatial structure and temporal evolution of energetic particle injections in the inner magnetosphere during the 14 July 2013 substorm event. *Journal of Geophysical Research: Space Physics*, *120*(3), 1924–1938. https://doi.org/10.1002/2014JA020872

Gkioulidou, M., Ukhorskiy, A. Y., Mitchell, D. G., & Lanzerotti, L. J. (2016). Storm time dynamics of ring current protons: Implications for the long-term energy budget in the inner magnetosphere. *Geophysical Research Letters*, *43*(10), 4736–4744. https://doi.org/10.1002/2016GL068013

Gkioulidou, M., Ukhorskiy, A. Y., Mitchell, D. G., Sotirelis, T., Mauk, B. H., & Lanzerotti, L. J. (2014). The role of small-scale ion injections in the buildup of Earth's ring current pressure: Van Allen Probes observations of the 17 March 2013 storm. *Journal of Geophysical Research: Space Physics*, *119*(9), 7327–7342. https://doi.org/10.1002/2014JA020096

Hamilton, D. C., Gloeckler, G., Ipavich, F. M., Kremser, G., Stüdemann, W., Wilken, B., & Stuedemann, W. (1988). Ring current development during the great geomagnetic storm of February 1986. *Journal of Geophysical Research*, *93*(A12), 14343–14355. https://doi.org/10.1029/JA093iA12p14343

Jordanova, V. K., Farrugia, C. J., Thorne, R. M., Khazanov, G. V., Reeves, G. D., & Thomsen, M. F. (2001). Modeling ring current proton precipitation by electromagnetic ion cyclotron waves during the May 14–16, 1997, storm. *Journal of Geophysical Research*, *106*(A1), 7–22. https://doi.org/10.1029/2000JA002008

Jordanova, V. K., Kozyra, J. U., & Nagy, A. F. (1996). Effects of heavy ions on the quasi-linear diffusion coefficients from resonant interactions with electromagnetic ion cyclotron waves. *Journal of Geophysical Research*, *101*(A9), 19771–19778. https://doi.org/10.1029/96JA01641

Keika, K., Nosé, M., Ohtani, S.-I., Takahashi, K., Christon, S. P., & McEntire, R. W. (2005). Outflow of energetic ions from the magnetosphere and its contribution to the decay of the storm time ring current. *Journal of Geophysical Research*, *110*(A9), A09210. https://doi.org/10.1029/2004JA010970

Khazanov, G., Gamayunov, K., Gallagher, D., Kozyra, J., & Liemohn, M. (2007). Self-consistent model of magnetospheric ring current and propagating electromagnetic ion cyclotron waves: 2. Wave-induced ring current precipitation and thermal electron heating. *Journal of Geophysical Research*, *112*(A4). https://doi.org/10.1029/2006JA012033

Kistler, L. M., Ipavich, F. M., Hamilton, D. C., Gloeckler, G., Wilken, B., Kremser, G., & Stüdemann, W. (1989). Energy spectra of the major ion species in the ring current during geomagnetic storms. *Journal of Geophysical Research*, *94*(A4), 3579–3599. https://doi.org/10.1029/JA094iA04p03579

Krimigis, S. M., Gloeclker, G., McEntire, R. W., Potemra, T. A., Scarf, F. L., & Shelley, E. G. (1985). The magnetic storm of September 4, 1984: A synthesis of ring current spectra and energy densities measured with AMPTE/CCE. *Geophysical Research Letters*, *12*(5), 329–332. https://doi.org/10.1029/GL012i005p00329

Li, X., Baker, D., Temerin, M., Cayton, T., Reeves, E., Christensen, R., et al. (1997). Multisatellite observations of the outer zone electron variation during the November 3–4, 1993, magnetic storm. *Journal of Geophysical Research*, *102*(A7), 14123–14140. https://doi.org/10.1029/97JA01101

Li, X., Hudson, M., Chan, A., & Roth, I. (1993). Loss of ring current O^+ ions due to interaction with Pc 5 waves. *Journal of Geophysical Research*, *98*(A1), 215–231. https://doi.org/10.1029/92JA01540

Li, X., Temerin, M., Baker, D. N., Reeves, G. D., & Larson, D. (2001). Quantitative prediction of radiation belt electrons at geostationary orbit based on solar wind measurements. *Geophysical Research Letters*, *28*(9), 1887–1890. https://doi.org/10.1029/2000GL012681

Liemohn, H. (1961). The lifetime of radiation belt protons with energies between 1 KeV and 1 MeV. *Journal of Geophysical Research*, *66*(10), 3593–3595. https://doi.org/10.1029/jz066i010p03593

Liu, W., Tu, W., Li, X., Sarris, T., Khotyaintsev, Y., Fu, H., et al. (2016). On the calculation of electric diffusion coefficient of radiation belt electrons with in situ electric field measurements by THEMIS. *Geophysical Research Letters*, *43*(3), 1023–1030. https://doi.org/10.1002/2015GL067398

O'Brien, T. P., & Moldwin, M. B. (2003). Empirical plasmapause models from magnetic indices. *Geophysical Research Letters*, *30*(4), 1152. https://doi.org/10.1029/2002GL016007

Ozeke, L. G., Mann, I. R., Murphy, K. R., Jonathan Rae, I., & Milling, D. K. (2014). Analytic expressions for ULF wave radiation belt radial diffusion coefficients. *Journal of Geophysical Research: Space Physics*, *119*(3), 1587–1605. https://doi.org/10.1002/2013JA019204

Roederer, J. G. (1970). *Dynamics of geomagnetically trapped radiation*. Springer.

Schulz, M., & Lanzerotti, L. (1974). *Particle diffusion in the radiation belts*. Springer.

Sheldon, R. B., & Hamilton, D. C. (1993). Ion transport and loss in the Earth's quiet ring current: 1. Data and standard model. *Journal of Geophysical Research*, *98*(A8), 13491–13508. https://doi.org/10.1029/92JA02869

Smith, P. H., & Bewtra, N. K. (1978). Charge exchange lifetimes for ring current ions. *Space Science Reviews*, *22*(3), 301–318. https://doi.org/10.1007/bf00239804

Sugiura, M. (1964). *Hourly values of the equatorial Dst for IGY* (Vol. 35, p. 945). Pergamon Press.

Tsyganenko, N. A., & Sitnov, M. I. (2005). Modeling the dynamics of the inner magnetosphere during strong geomagnetic storms. *Journal of Geophysical Research*, *110*(A3), A03208. https://doi.org/10.1029/2004JA010798

Tu, W., Elkington, S. R., Li, X., Liu, W., & Bonnell, J. (2012). Quantifying radial diffusion coefficients of radiation belt electrons based on global MHD simulation and spacecraft measurements. *Journal of Geophysical Research*, *117*(A10), A10210. https://doi.org/10.1029/2012JA017901

Tu, W., Li, X., Chen, Y., Reeves, G. D., & Temerin, M. (2009). Storm-dependent radiation belt electron dynamics. *Journal of Geophysical Research*, *114*(A2), A02217. https://doi.org/10.1029/2008JA013480

Tu, W., Xiang, Z., & Morley, S. K. (2019). Modeling the magnetopause shadowing loss during the June 2015 dropout event. *Geophysical Research Letters*, *46*(16), 9388–9396. https://doi.org/10.1029/2019GL084419

Turner, D. L., Angelopoulos, V., Morley, S. K., Henderson, M. G., Reeves, G. D., Li, W., et al. (2014). On the cause and extent of outer radiation belt losses during the 30 September 2012 dropout event. *Journal of Geophysical Research: Space Physics*, *119*(3), 1530–1540. https://doi.org/10.1002/2013JA019446

Williams, D. J. (1981). Ring current composition and sources: An update. *Planetary and Space Science*, *29*(11), 1195–1203. https://doi.org/10.1016/0032-0633(81)90124-0

Zhao, H., Li, X., Baker, D. N., Fennell, J. F., Blake, J. B., Larsen, B. A., et al. (2015). The evolution of ring current ion energy density and energy content during geomagnetic storms based on Van Allen Probes measurements. *Journal of Geophysical Research: Space Physics*, *120*(9), 7493–7511. https://doi.org/10.1002/2015JA021533